

GT2011-46558

## FURTHER INVESTIGATION OF THE INFLUENCE OF REAL-WORLD BLADE PROFILE VARIATION ON THE AERODYNAMIC PERFORMANCE OF TRANSONIC NOZZLE GUIDE VANES

J. Ilott<sup>1</sup>, A. Asghar<sup>1</sup>, W.D.E. Allan<sup>1</sup> and R. Woodason<sup>2</sup>

<sup>1</sup>Royal Military College of Canada

Kingston, Ontario Canada

<sup>2</sup>StandardAero Ltd

Winnipeg, Manitoba Canada

### ABSTRACT

This paper addresses the issue of aerodynamic consequences of variations in airfoil profile. An analysis of new and repaired airfoils was used to synthesize profiles representative of specific repair types. Five variations of a reference new low pressure turbine vane were obtained by changing the characteristic parameters of trailing-edge tweaking and laminate-repair methods used to refurbish turbine vanes. Flow visualization of shock structure and total pressure measurements were made by experimentation in a cascade rig and by calculations through Computational Fluid Dynamics (CFD). The performance of the modified profiles was compared with that of the reference new vane. The total pressure losses increased when the profile was bent at the trailing edge towards the pressure side. The losses for synthesized laminate repair profiles increased with an increase in the thickness of laminate repair. The numerical results were used to supplement experimental results in cases where the experimental conditions were not representative of typical design operating conditions.

### NOMENCLATURE

$b$	span
$c$	true chord length
$M$	Mach number
$P$	pressure
$Re$	Reynolds number
$s$	pitch
$v$	velocity
Greek	
$\beta$	metal angle of blades

$\gamma$  stagger angle

$\rho$  density

### Subscripts

1 values at cascade inlet

2 values at cascade exit

0 total pressure

s static pressure

$x$  axial direction

$y$  pitchwise direction

### Abbreviations

CAD Computer aided design

CFD Computational fluid dynamics

CCD Charged couple device

LP low pressure

LPT low pressure turbine

LTE laminate trailing edge repair

NGV nozzle guide vanes

NV new vane

PS pressure surface

SS suction surface

TE trailing edge

TTE tweaked trailing edge

### INTRODUCTION

The performance of the turbine section in a gas turbine engine plays a major role in the overall efficiency of the engine and is strongly dependent on the profile losses, secondary losses and clearance (or leakage) losses of the nozzle guide vanes (NGVs) and rotor blades of turbine. During a gas turbine engine

overhaul or repair, the blade profile of the repaired turbine blades may be unintentionally altered, thereby negatively affecting the overall engine performance. This contributes to the cost of maintenance since engine overhaul facilities must address these issues with little supporting technical information. In earlier studies [1,2], a conspicuous change in flow pattern was observed due to noticeable variations in airfoil profile. However, a trend in pressure loss was not substantiated, partly due to the limited number of random off-design profiles tested.

The effect on turbine performance of the blade profile has been studied experimentally since the advent of gas turbines and computationally in recent decades; both areas of study can be found in many introductory books on gas turbines [3,4,5,6]. Two dimensional cascade studies of turbine blades through either the test rig or computations provide a valuable tool for estimating the pressure loss coefficient of the 2D blade profiles. Various aspects of the transonic turbine blade profile such as leading and trailing edge configurations, surface curvature and aspect ratio have been studied over the last few decades to improve the understanding of loss mechanisms and methods of performance estimation [7,8,9,10]. The presence of trailing edge shock structure in transonic turbines produces additional losses [9,11,12]. The mechanism of losses associated with the trailing edge flow and shock structure is discussed in some detail by Denton and Xu [13].

To further investigate the aerodynamic effects of repair processes commonly applied to NGVs, two methods of investigation were adopted here. First, experiments were conducted in a transonic 2D cascade rig in order to test blades with profiles of a reference new vane and five variants. The variants profiles were synthesized after analyzing typical profile defects. In the second method, a computational approach was applied to obtain a numerical solution of the flow about a cascade of the same six profiles. CFD simulations were used to supplement and complement the test rig data, particularly for those parameters which were not available in experiments or for which experiments were limited.

Most gas turbine engines are overhauled after a certain number of hours of service. During maintenance, turbine nozzle guide vanes may be repaired, depending upon the nature and extent of deterioration. After an engine is overhauled and reassembled, it is common practice to perform an acceptance test in a test bed. Sometimes engine performance requirements are not met; one possible cause is the condition of the turbine nozzle guide vanes. Although steps are taken to restore original blade profiles during NGV repair, some deviations are inevitable. In this paper, a parametric study of repaired vane profiles was conducted to understand the influence of selected repairs on the performance of refurbished turbines.

### **NGV Repair**

A survey of turbine NGV profiles found after engine maintenance suggested the following key fault modes and reasons for airfoil alterations:

**Laminate Repair** One repair scheme to treat thinning or cracking near a vane's trailing edge involved brazing a preformed laminate on the suction surface. Despite a blending operation intended to merge the original suction surface with the laminate, suction surface curvature is invariably altered and an increased trailing edge thickness could occur.

**Tweaking** In the repair industry, hot striking, or mechanically bending the trailing edge of an airfoil up or down is an industry practice used to make small adjustments to an NGV's flow capacity. By definition, these procedures alter the aerodynamic profile of the part.

**Leading Edge Modification** Leading edge profiles may be altered either by erosion during engine operation or may be due to repair by welding local cracks. The off-design geometry may affect both the leading edge radius and the effective flow incidence angle.

**Suction Surface Distortion** Undulating suction surface profiles have been observed in areas that would not be accessible for rework or repair. The specific cause is not known. Thermal distortion linked to the vane's internal cooling features or manufacturing variation are both suspected.

## **EXPERIMENTAL SETUP**

To study the effect of profile modifications due to repair, two dimensional linear cascade tests were carried out. Firstly, flow visualization of shock and expansion waves was carried out using schlieren imagery in experiments and axial density gradient calculations in computations. Secondly, downstream total pressure and flow angle were determined, both experimentally and numerically. Cascade experiments were performed in the transonic wind tunnel at the Royal Military College of Canada (RMCC). Air at atmospheric pressure and temperature was drawn through a contraction into the wind tunnel and was discharged into a vacuum tank downstream of the test section. Details about the wind tunnel and the experimental setup are described in a previous paper [14] and are also available in [1]. Only cascade rig details which are relevant to the present investigation are described here.

The cascade was constructed using one set of blades with a mean line profile of a reference new vane of a low pressure (LP) turbine of an in-service turboshaft engine and five variants of representative repaired profiles of the same new vane. The new vane profile was obtained by measuring the airfoil profile of a new NGV. The modification of the vane profile due to repair was modeled by incorporating the effect of two NGV repair schemes on cascade blades. It was achieved by changing the profile of the NV airfoil in a manner similar to the repaired NGV. Further, by changing the defining parameter of each of these repair schemes, various iterations on the profile modification were carried out. The first repair type was *tweaking* the trailing edge at the 75% chord of the new vane. The parametric adjustment used was a 3-degree bending of the trailing edge (see Fig. 1.) of the new vane airfoil; one test article was bent towards the pressure side (-3 degrees) and another towards the suction side (+3 degrees).

The second parametric study simulated geometric alterations imposed by laminate repairs. This led to three successive increases in the reference NV trailing edge thickness from 75% chord to the trailing edge (see Fig. 2). The thickness was increased by 25%, 50%, and 75% for three test articles. The original profile and laminate repair were blended from 65% chord to 85%, 87.5% and 90% chord, respectively for the 25%, 50% and 75% thickness laminate repairs. Table 1 provides the nomenclature and details of parameters that were changed.

**TABLE 1: SUMMARY OF AIRFOIL PROFILES**

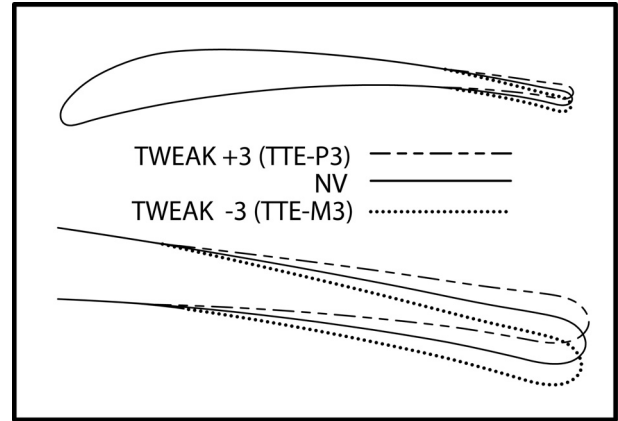
Abbreviation	Airfoil / Repair Scheme	Parameter Changed
NV	Reference new vane	None
TTE-M3	Tweaking of trailing edge.	3-degree bent towards the pressure side (-3°)
TTE-P3	Tweaking of trailing edge.	3-degree bent towards the suction side (+3°)
LTE-25	Laminate repair at trailing edge.	TE thickness 25% greater than NV TE thickness
LTE-50	Laminate repair at trailing edge.	TE thickness 50% greater than NV TE thickness
LTE-75	Laminate repair at trailing edge.	TE thickness 75% greater than NV TE thickness

The cascade blades were fabricated from Accura Bluestone™ nano-composite plastic using solid-state lithography. The dimensional tolerance of the manufacturing process was 0.2 mm (approximately 1.5% of the nominal throat size). The surface of the manufactured blade used in the cascade was qualitatively smooth.

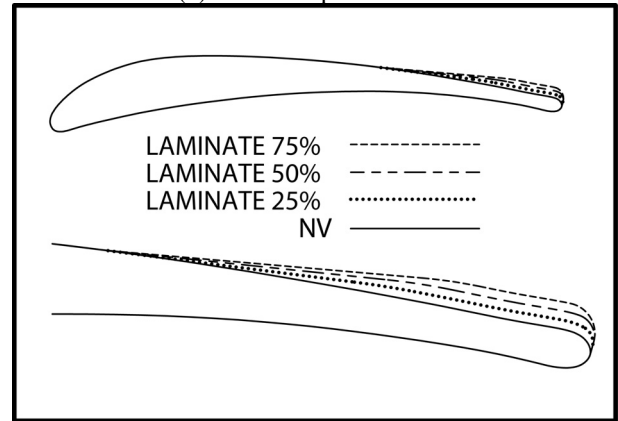
The relevant geometry of the reference NV airfoil and cascade configuration is given in Table 2. Further details of the cascade operating parameters and measurement location are shown in Figure 2. In the cascade, five flow passages were formed by four blades and two profiled side walls, also shown in Fig. 2. The cascade operating parameters were kept the same as the NGVs, the profiles of which were used for the manufacturing of the cascade blades. The upper and lower side walls upstream of the cascade were inclined with respect to the cascade to make the desired flow angle equal to the blade inlet angle. The flow entered the cascade with a zero incidence and at subsonic Mach numbers, accelerating to transonic exit flow through the cascade.

The cascade exit condition was set by inclining the upper side wall by 66° with respect to the cascade axis, while the lower side wall was inclined by approximately 62° with respect

to the cascade axis. The reflection of the exit shocks into the cascade was suppressed using a perforated tailboard on the lower side wall, downstream of the trailing edge of the pressure-surface profile of the last flow passage.



(a) Tweak Repair Profiles



(b) Laminate Repair Profiles

**FIGURE 1: SIX PROFILES OF CASCADE BLADES**

The static pressure across the inlet and exit was measured three-quarters of the axial chord upstream of the cascade inlet and half the axial chord downstream of the cascade exit (see Fig. 2). The shock pattern in the cascade was visualized using a Z-type schlieren system. These images were recorded directly with a RedLake (Model PCI 8000 S) video camera, which had a CCD of 658 × 496 pixels. The video was captured at 60 frames per second using an exposure time of 1/1200 s. Total pressure measurements were made ½-axial chord downstream of the cascade exit (see Fig. 2) at the midspan height of the blade and in the middle passage of the cascade using a 7-hole probe [1]. The estimated uncertainty in the total pressure ratio was approximately 1%.

**TABLE 2: GEOMETRY OF NV-AIRFOILS AND CASCADE OPERATING PARAMETERS**

Parameter		NV	unit
True chord	$c$	53.3	mm
Axial chord	$c_x$	32.6	mm
Pitch	$s$	35.5	mm
Span	$b$	50.8	mm
Throat opening	$t$	14.6	mm
Solidity	$c/s$	1.50	[-]
Aspect ratio	$b/c$	0.95	[-]
Stagger angle	$\gamma$	52.6	deg
Inlet metal angle	$\beta_1$	31	deg
Exit metal angle	$\beta_2$	66	deg

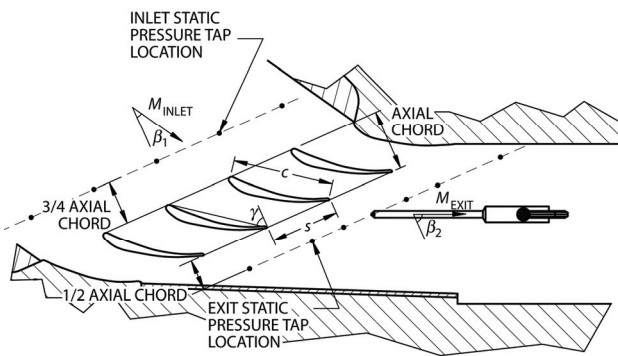


**FIGURE 2: CASCADE PARAMETERS AND PRESSURE MEASUREMENT LOCATIONS**

**FLOW CONDITIONS**

Since blade profiles of low pressure turbine (LPT) NGVs were used in the experiments, the flow in the cascade was established using the operating parameters of the same nozzle guide vanes. Since the NGVs of the turbine were operated at choked flow condition at design point, the cascade design exit condition was also set at the choked flow condition of NV airfoils. The average inlet flow Mach number was 0.30. The inlet flow angle was not measured; however, it was confirmed by surface flow visualization that the inlet flow was essentially parallel to the upper and lower side wall at the entrance. The flow at the exit was transonic at an average Mach number of  $M > 1.0$ . The Reynolds number based on the true chord was found to be  $3.5 \times 10^5$ . The turbulence intensity in the test section was measured by hotwire and found to be 0.5%.

Note that the turbulence in the engine is substantially higher than that of the cascade tests; however, because the objective of the present paper was to investigate the effect of the profile variation on the performance, the effect of turbulence was not considered.

**COMPUTATIONAL ANALYSIS**

ANSYS-CFX version 12.1 was used to simulate the flow in the cascade. The computational domain was constructed using the

same CAD models which were used for the manufacturing of the test rig blades and cascade. Figure 3 illustrates the computational domain, and blocking structure that were used. The inlet boundary was placed  $1\frac{3}{4}$  axial chord lengths upstream and the outlet of the domain was placed  $3\frac{1}{2}$  axial chords downstream. One-to-one (1:1) translational periodic boundaries were applied in the pitch-wise direction. A hexagonal mesh was generated using ANSYS-ICEM version 12.1.

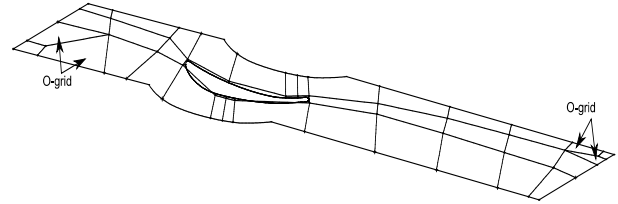
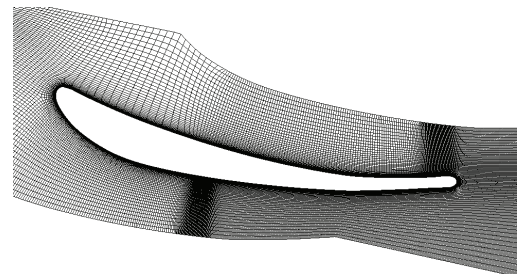
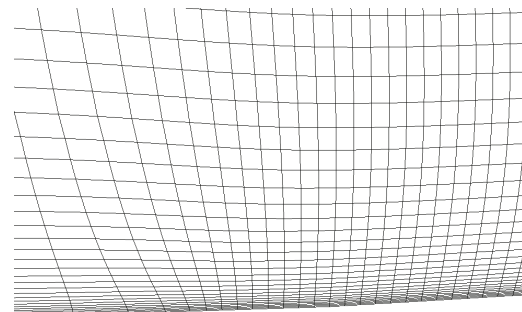


**FIGURE 3: COMPUTATIONAL DOMAIN**

A hybrid H-O multiblock mesh topology was constructed using H-blocks with  $\frac{1}{4}$  O-grid blocks placed around two diagonally opposite corners (as shown in Fig. 3) to allow alignment of the H-blocks with the flow direction while maintaining 1:1 periodicity. An O-grid block was used to allow refinement of the grid spacing normal to the airfoil surface. The grid spacing was reduced in the streamwise direction in the regions where shocks were expected which included the blade-to-blade throat and the trailing edge region, Fig. 4(a) shows the mesh used around the airfoil. A fine mesh was required in the entire downstream region to satisfy the 1:1 periodic boundary requirement. Figure 4(b) shows the fine grid spacing used in the near wall region of the airfoil and the fine streamwise spacing in the trailing edge region.



(a) Around the Airfoil



(b) Close to the Surface near the Expected Shock

**FIGURE 4: MESH REFINEMENT**

To ensure that a grid-independent solution had been obtained, two results of interest were compared for two meshes. Both the minimum total pressure ratio measured in the wake and the mass flow rates through the domain were compared. The results of the grid-independence evaluation are shown in Table 3. These results indicate that a grid-converged solution was obtained for the 94749 node mesh.

**TABLE 3: TESTS FOR GRID CONVERGENCE**

Number of Nodes	Minimum ( $P_{02}/P_{01}$ )	% Change
94749	0.8199	0
375368	0.8243	0.5

Number of Nodes	Mass Flow Rate(kg/s)	% Change
94749	0.002184	0
375368	0.002182	0.09

The fluid flow was simulated using ANSYS-CFX to solve the Reynolds-Averaged Navier-Stokes (RANS) equations for the fluid domain. The presence of inclined shock and expansion waves required a very low aspect ratio grid in the vicinity of the trailing edge since the mesh could not be made orthogonal to the steep gradients in this region. In the boundary layer refinement region, the aspect ratio became very high with the node spacing much smaller in the direction parallel to the shocks, than in the direction normal to the shocks. It is common to observe the *carbuncle* problem, a numerical instability that is transverse to the shock, under these conditions [15,16]. Although this numerical phenomenon is more common in inviscid simulations, it can also occur for viscous cases [15,16]. To address this and other numerical stability problems that can occur in high speed flows, the High Speed Numerics feature of ANSYS-CFX was enabled. This feature modifies the solver numerics by introducing additional dissipation at the shocks, applying an upwind advection blending in the shock region and modifying the relaxation factors for the advection blending and flow gradients in the shock region [15]. The convergence criteria for a solution of the hydrodynamic variables (mass and momentum) were based on the reduction to less than  $10^{-5}$  of the normalized residuals, providing an approximate reduction of the solution error of five orders of magnitude.

The closure of the RANS equations was achieved using a two-layer, two-equation shear stress transport (SST) turbulence model developed by Menter [17]. The SST model provides major improvement in the prediction of adverse pressure gradient flows and in the wake-region flow of the blades.

Numerical simulations were performed nominally at the same operating conditions as those of the cascade in the experiments. At the inlet of the domain, standard atmospheric pressure (total), static temperature and flow direction were

specified. At the outlet of the domain, static pressure was imposed as the boundary condition. However, the measured static pressure was not specified as the exit condition. Instead, an incremental decrease in the back pressure was undertaken from a pressure at which the cascade flow was unchoked to a lower back pressure when the fully choked flow condition was established in the cascade. This procedure of identifying the choked flow condition is demonstrated in Fig. 5 for the TTE-P3 and LTE-75 airfoils.

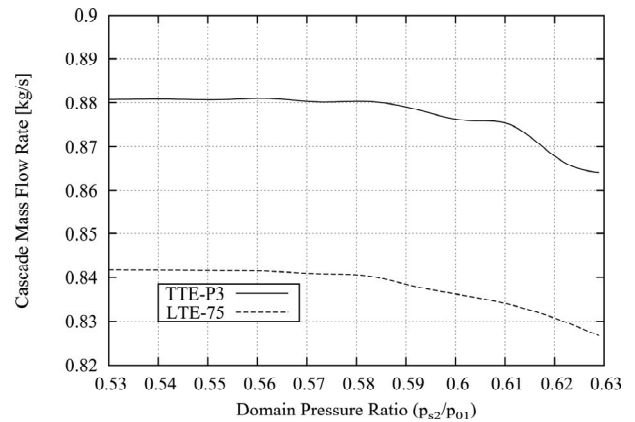


**FIGURE 5: COMPUTED CHANGES IN MASS FLOW WITH BACK PRESSURE FOR TTE-P3 and LTE-75**

## RESULTS AND DISCUSSION

During the cascade testing reported in [1,14], it was identified that even small but noticeable differences in the airfoil profiles could cause substantial degradation in performance. For a more systematic study of profile modification due to repair, two repair schemes were chosen and a parametric study was carried out. The observed flow field and total pressure survey for these repair schemes are given in the following sections and are compared with the reference new vane. The results reported in this section are mainly for the middle passage of the cascade, which in essence simulates the infinite cascade.

### Flow Visualization

In the present study, the main investigative tools were the observation of shock pattern and the determination of total pressure ratio at the cascade exit. In the experiments, schlieren flow visualization and in computations, axial density gradient, were used to observe the shock-flow pattern. These observations are shown in Figs. 6 and 7 for the two repair schemes along with the reference new vane. The deviations of shock pattern for TTE airfoils from the NV airfoil are seen in Fig. 6. The schlieren flow pattern showed nominally periodic flow for NV and TTE-M3 airfoils but not for TTE-P3 airfoils; however, for TTE-P3 the flow in the middle (third from top) was considered as representative of the infinite cascade flow. The flow pattern for TTE-M3 showed an increase in Mach number as indicated by a relatively large downstream inclination of the shock wave. The higher Mach number flow was predictable since the throat area was decreased in the

passage due to mechanical TE bending towards the pressure surface ( $-3^\circ$ ). The flow was choked in the blade passage and then again turned sonic downstream of the exit. The downstream sonic condition was achieved due to a reduction of the effective flow area by the TE wake flow. The passage shock interacted with the suction surface of the neighboring blade and reflected (due to higher Mach numbers) towards the TE wake. The presence of a thick boundary layer on suction surface was observed through the diffused flow at the location where shock interacted with the suction surface boundary layer. The shock pattern at the trailing edge clearly indicated the presence of two shocks: one originating right at the trailing edge and the other emanating from the wake.

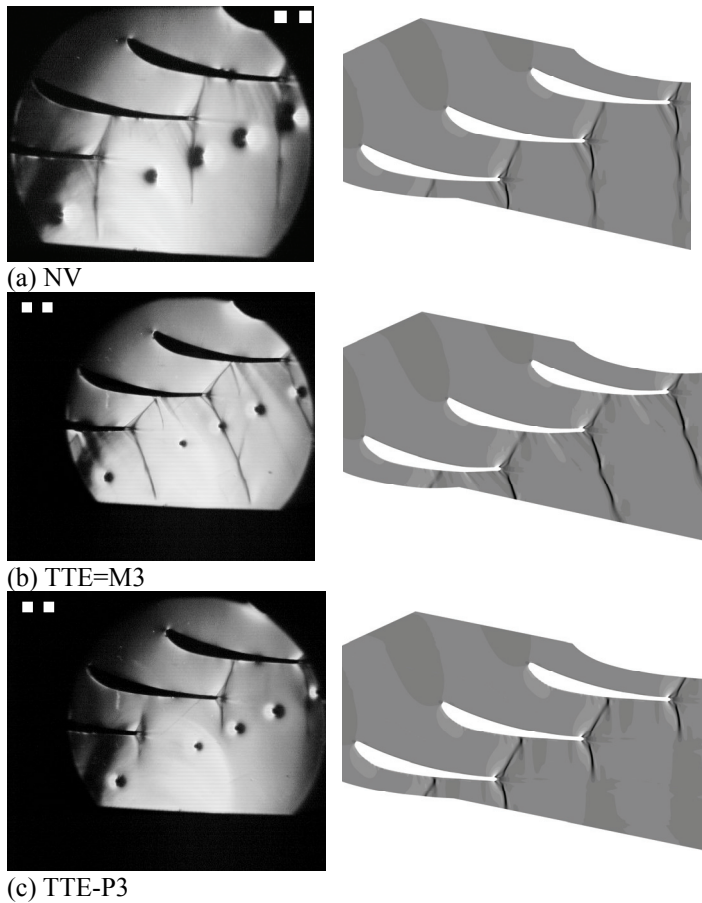


**FIGURE 6: SCHLIEREN IMAGES AND COMPUTED AXIAL DENSITY GRADIENT OF SHOCK FLOW PATTERN FOR NV and TTE PROFILES**

The flow pattern for TTE-P3, although somewhat less interesting with respect to shock waves, was also different from the NV airfoil. The flow in the middle passage (3rd passage from top) was not completely choked in the passage; however, the flow finally became sonic near the trailing edge, as indicated by the weak shock structure. The Mach number near the trailing edge was lower due to a widening of the throat area

in the blade passage due to mechanical bending of the trailing edge towards the passage on the suction side of the blade.

The cascade flow for various thicknesses of laminate repair test articles was different for each of the airfoils as well as from the NV airfoil flow as shown in Fig. 7.

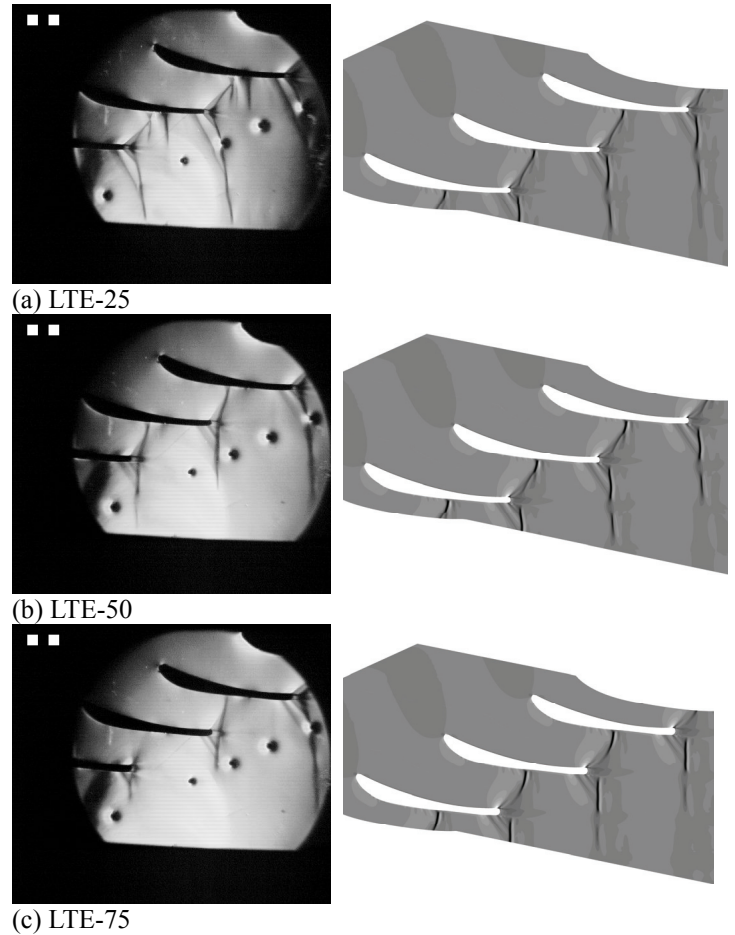


**FIGURE 7: SCHLIEREN IMAGES AND COMPUTED AXIAL DENSITY GRADIENT OF SHOCK FLOW PATTERN FOR LTE PROFILE**

In the experiments, the flow was nominally periodic for LTE-25 and LTE-50 airfoils but not for LTE-75; however, for LTE-75 the flow in the middle (third from top) was considered representative of the infinite cascade flow. The flow was choked in the middle cascade passage for the LTE-25 and LTE-50 airfoils, but not for the LTE-75. The shock flow on the LTE-25 airfoil was different from the NV airfoil and indicated a higher Mach number as seen by the downstream inclination of the shock wave. The shock flow for the LTE-50 profile was to some extent similar to the NV airfoil. For the LTE-75 profile, sonic condition was reached downstream of the cascade exit due to a reduction of the effective flow area between the laminate repair (on suction side) and the slow-moving wake. The boundary layer on the LTE-25 airfoil indicated by the

diffused flow at the shock boundary layer interaction appeared to be thicker than the boundary layer on the TTE-M3 (as described above). The effect of laminate repair was also noted at the 85% chord by the presence of weak oblique shock waves. For LTE-75, this effect was even stronger as noted by the shock structure on the suction side of the third blade from the top. In the schlieren images, widening of the base flow was also observed behind the trailing edge. The axial density gradient obtained through CFD showed similar behaviour to that exposed by the schlieren technique in the complimentary experiments for TTE-M3, LTE-25 and LTE-50 airfoils. However, for TTE-P3 and LTE-75 the computed axial density gradients were not the same as the schlieren images in the experiments. In the experiments, the flow was not completely choked in the middle passage for TTE-P3 and LTE-75 due to limitation in the cascade test section. However in CFD, both choked and unchoked flows could be obtained by adjusting the back pressure at cascade exit. Figures 6(c) and 7(c) show the computed axial density gradient for the just choked flow condition in TTE-P3 and LTE-75. In the CFD results, the unchoked flow corresponded to higher back pressure (not shown here). As described with respect to Fig. 5, the higher back pressure would also correspond to a lower mass flow rate.

Note that although the CAD models used for the manufacturing of the blades in the experiments and for generating the CFD domain were the same, the experimental setup was slightly different from the CFD setup due to the method of supporting the blades in the acrylic endwalls. The weak oblique shock observed in the experiments, but not in the CFD, for TTE-M3 and LTE-25 airfoils were exactly at the position where the blades were attached to the wall by small tabs or bosses. A small gap at this location will cause this oblique shock at higher Mach numbers.

### Surface Mach Number

The surface Mach number for the six airfoils (see Fig. 8) showed the effect of profile variation and shock impingement on the suction surface. For the TTE-M3 profile, an increase in Mach number near the 75% chord as shown in Fig. 8(a) (expanded view in Fig. 8(b)) was obtained due to flow acceleration along the bent TE, while in the TTE-P3 profile the opposite effect was observed. The effect of camber change due to the bending of the TE is also seen in Fig. 8(a) on the suction side LE as well as on the pressure side of the airfoils by the modified loading for TTE-M3 and TTE-P3 airfoils. For LTE airfoils, the effect of laminate repairs can be seen from 65% chord to the TE (Fig. 8(c) (expanded view in Fig. 8(d))). Very close to the TE (90% chord), the surface pressure indicated flow separation, contributing to higher pressure losses. The flow on the suction side LE up to 50% chord and the pressure side essentially remained unchanged for all the LTE test profiles (Fig. 8(c)).

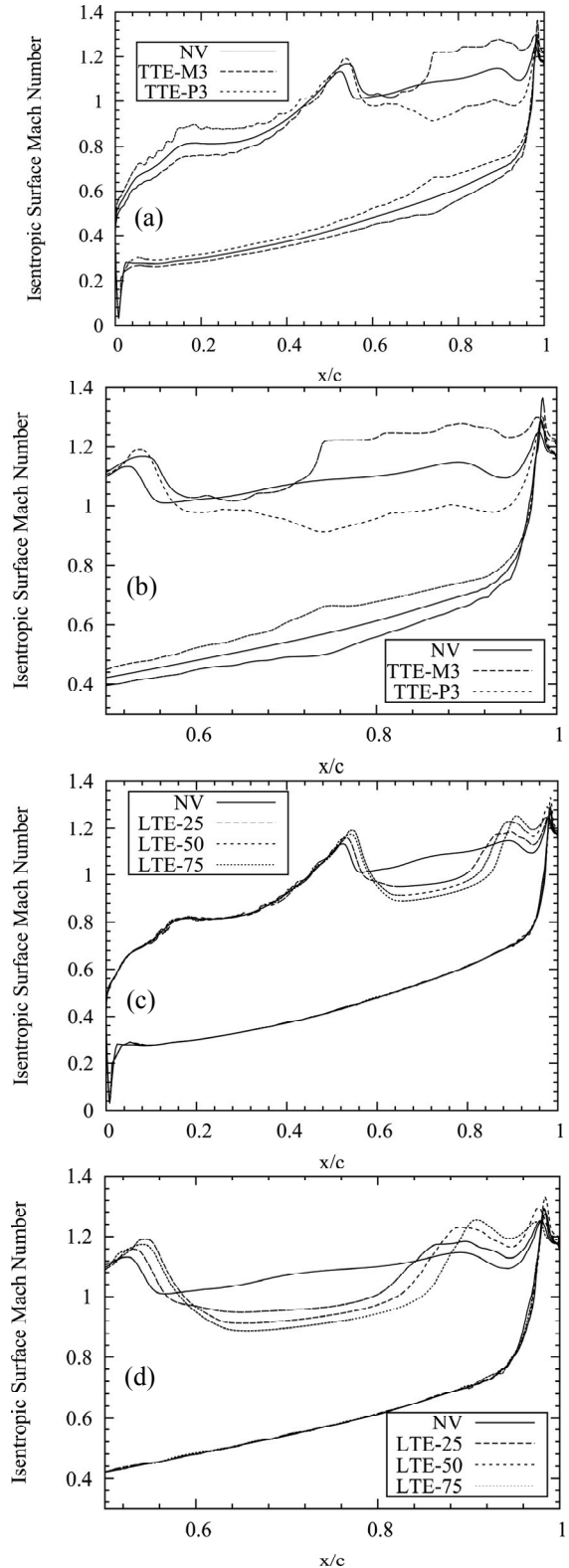


**FIGURE 8: COMPUTED SURFACE MACH NUMBERS OF NV, TTE, and LTE AIRFOILS**

**Cascade Mach number**

The Mach number in the cascade, as obtained by CFD, is given in Fig. 9 for the NV and TTE profiles. The Mach number provided a quick method of identifying choked flow and strength of shock, thereby indicating the nature of losses due to transonic flow. The computations showed the positions of Mach 1 flow and its downstream development. For all of the profiles, the sonic condition was attained at two locations, one in the passage and the other between the suction surface and TE wake.

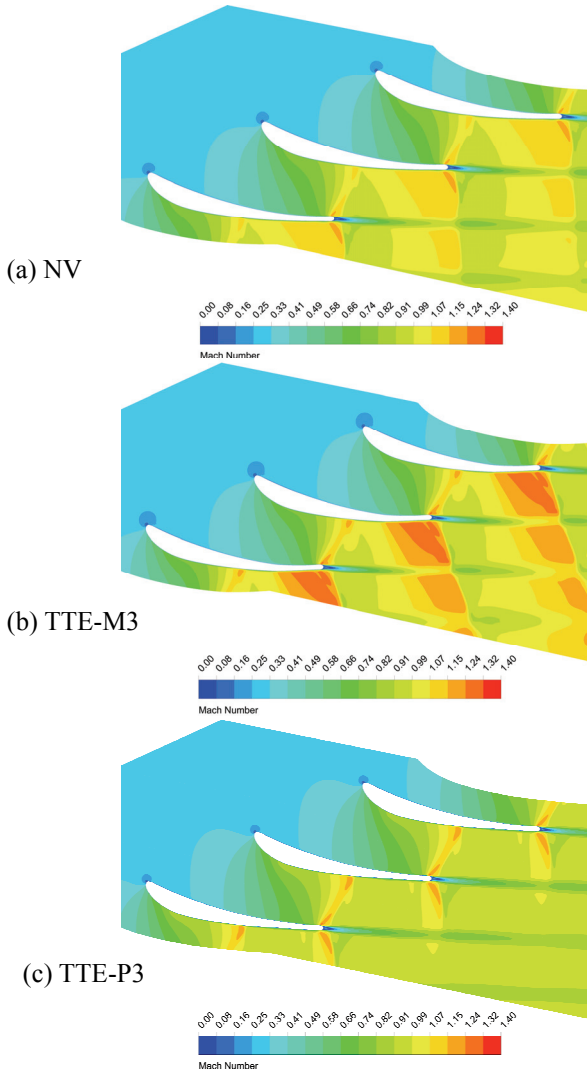


**FIGURE 9: COMPUTED MACH NUMBER FOR NV AND TTE AIRFOILS**

As seen in Fig. 10, Mach numbers for the LTE airfoils indicated higher Mach flow for LTE-25 airfoils but a progressively lower Mach number flow for the LTE-50 and LTE-75 profiles. This indicates that more losses would be expected between the wakes for LTE-25.

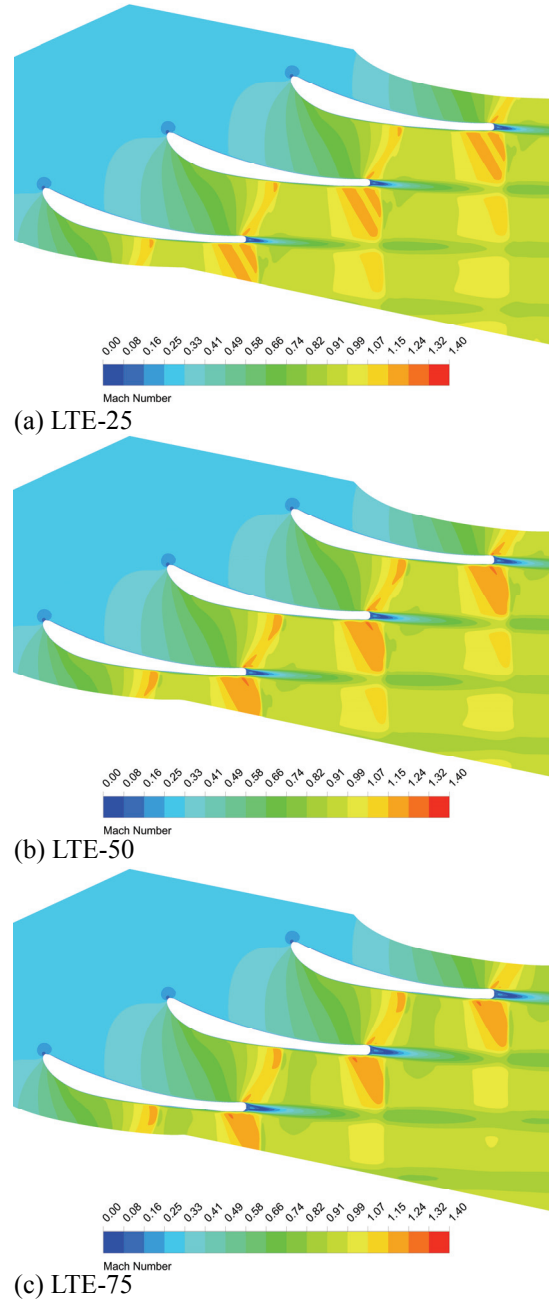


**FIGURE 10: COMPUTED MACH NUMBER FOR LTE AIRFOILS**

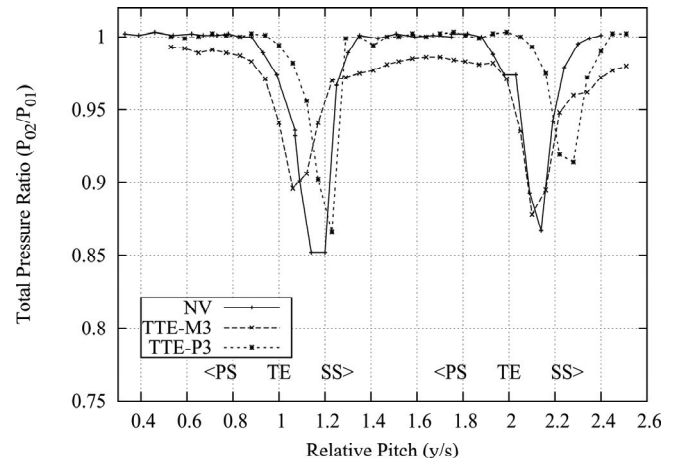
**Exit Total Pressure Ratio**

The isentropic total pressure ratio at the cascade exit for the NV and TTE airfoils, taken 1/2 axial chord downstream from the trailing edge, is shown in Fig. 11(a) for flow measurements and in Fig. 11(b) for the computations. The effect of profile changes on the total pressure ratio was clearly visible in both plots. In the experiments (see Fig. 11(a)), the shift in wake position for the TTE airfoils from the NV airfoil was due to bending of the

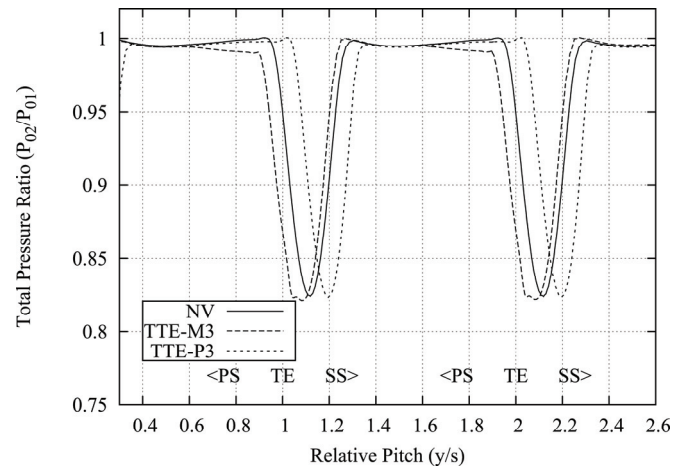
TE by  $\pm 3$  degree. The drop in total pressure ratio for TTE-M3 was large compared to that of the NV airfoil, especially between the wakes. This clearly showed the effect of multiple shocks on losses, and thus the effect of profile modification on the performance. However, the total pressure ratio between the wakes for TTE-P3 remained similar to NV, mainly due to unchoked flow in the cascade of the experiment and due to just choked flow in the CFD. The wake of TTE-M3 was wider than that of the TTE-P3. The total pressure ratio obtained in computations, in general, showed similar trends to those obtained in experiments, such as shifting of wake due to bending in TTE airfoils. However, CFD clearly showed that the losses in the wake were higher and almost unchanged for both the TTE-M3 and TTE-P3 blades. Note that the computed pressure losses for TTE-P3 are for choked flow in the cascade, whereas for experiments it was for unchoked flow. For TTE-M3, the computation did show increased losses in the mid-passage area, but in general, in the mid-passage area, the computed pressure ratio was higher than that in the experiments. It was however somewhat similar to the behaviour observed in previous experimental work reported in [2].

For the LTE-airfoils, as shown in Fig. 12(a) for the experiments, the total pressure ratio in the passage dropped in comparison with that of the NV airfoil. The drop in total pressure ratio between the wakes was relatively higher for the LTE-25 than for the LTE-75 airfoil. This was due to the presence of strong shock flow on LTE-25 airfoil. The pressure ratio for LTE-75 was close to NV in the mid-passage area, but decreased rapidly because of the wake widening due to thick laminates. As expected, wakes were progressively wider for the LTE-25 to LTE-75 airfoils, consistent with increased TE thicknesses thereby contributing to higher wake losses.

In general, the total pressure ratio obtained in the computations for the LTE airfoils showed a similar trend as those obtained in the experiments, such as widening of the wake with an increase in laminate repair thickness and increased losses in the mid passage area. The CFD results clearly showed that the losses in the wake increased with the increase in the laminate repair thicknesses. The shift in the wake region towards the suction side was also observed in the computations. However, similar to TTE airfoils, the CFD again clearly showed that the losses in the wake were higher than those observed in the experiments. Note that the computed total pressure ratio for LTE-75 airfoils was for choked flow, but for experiments it was for unchoked flow.

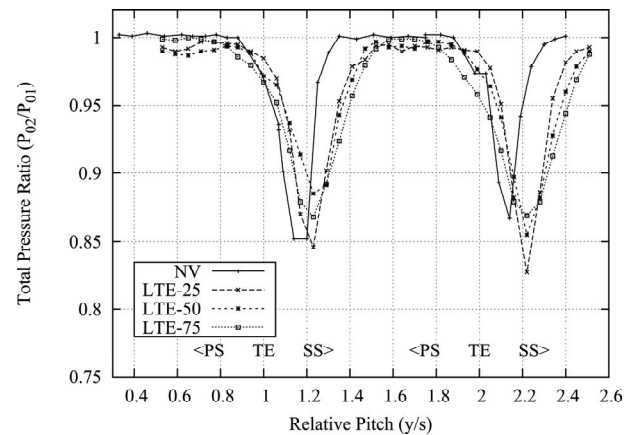


(a) Experiments



(b) Computations

**FIGURE 11: TOTAL PRESSURE DISTRIBUTION FOR NV AND TTE PROFILES**



(a) Experimental

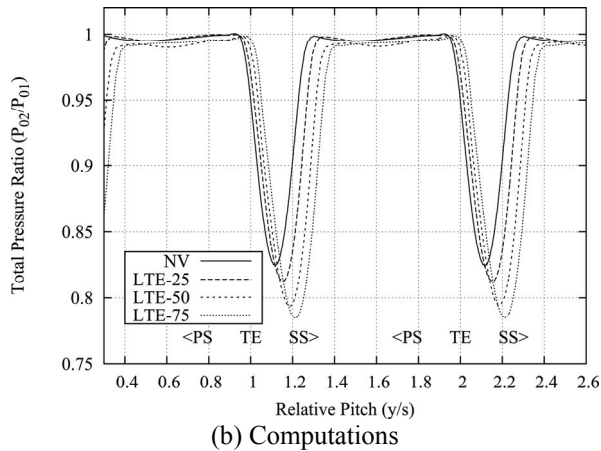


**FIGURE 12: TOTAL PRESSURE DISTRIBUTION FOR NV AND LTE PROFILES**

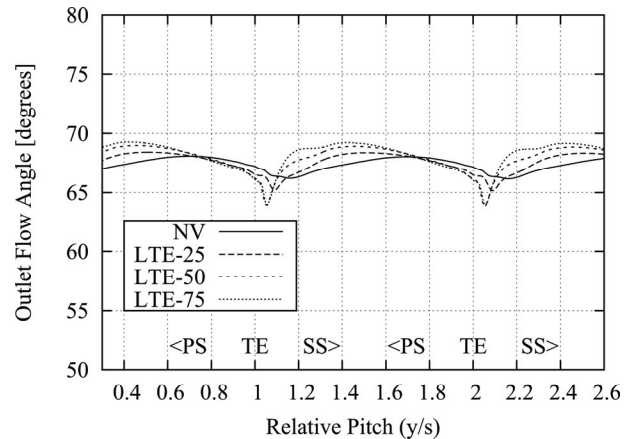


**FIGURE 14: COMPUTED OUTLET ANGLE FOR NV and LTE PROFILES**

### Outlet Flow Angle

The computed cascade outlet angles for the airfoils are shown in Figs. 13 and 14. The effect of profile changes on outlet angle is clearly visible in the plots. The computed outlet angles were not compared with the measured angles, because the measured angles showed very little change. The reason for this could be explained by the fundamental difference between the cascade rig and the CFD setup. In the cascade rig, the upper and lower sidewalls fixed the outlet angle to  $66^\circ$  whereas the CFD boundary condition set no restriction on the outlet angle and thus the exit flow was free to deviate from the actual physical limitation. Note that for the TTE airfoils (Fig. 13), the outlet angle in computations changed by 3 degrees, due to the bending of the TE by precisely that much. For the LTE airfoils (Fig. 14), the outlet flow angle in the computations shifted by 2 to 3 degrees, due to laminate repair. The shift increased from LTE-25 to LTE-75. The computed changes in the outlet flow angles with the variations in the airfoil profiles were mainly due to the modified TE metal angles of the blades.

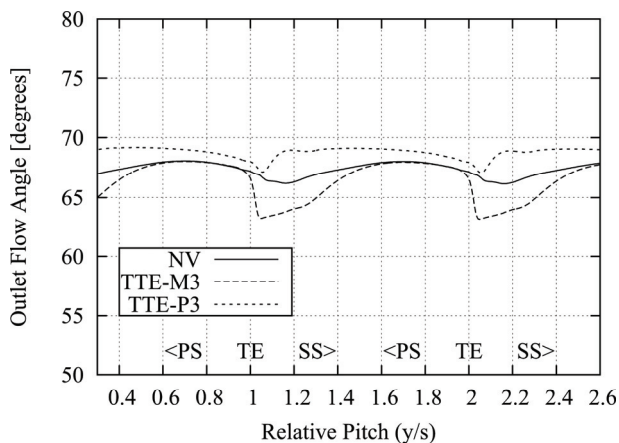


**FIGURE 13: COMPUTED OUTLET ANGLE FOR NV and TTE PROFILES**

The cascade exit losses calculated using the integration of the measured and computed total pressure are compared in Tables 4 and 5. For the TTE airfoils, the losses obtained through CFD showed the increase (as compared to the NV airfoil) due to the bending of the TE. The losses were higher in both the measurements and the computations for the TTE-M3 airfoil than for the TTE-P3 due to higher shock losses on the TTE-M3 airfoil. For the TTE-P3 airfoil, there were some discrepancies (see % change in Table 4) between the experiments and the computations in the trend for the losses, mainly due to the unchoked flow for TTE-P3 airfoils in the experiments and choked flow in the cascade of the computations, a phenomenon that was described earlier in this paper. Note that the losses for the TTE-P3 airfoils in the experiments were measured for the unchoked flow. For the LTE airfoils, the losses monotonically increased as the laminate repair thickness increased, most likely due to increased wake losses. However, this increase was more incrementally uniform in the computations than in the experiments. The relative percentage change in the pressure losses due to the profile variation (as compared to NV airfoil) were not in agreement with the measurements and computations, which may be due to the flow phenomena in the wake and boundary layer which may be poorly simulated by the turbulence model.

**Table 4: AREA-AVERAGED PRESSURE LOSS COEFFICIENTS FOR NV AND TTE AIRFOILS**

Airfoil	Computation (Change %)	Measurements (area-averaged) (Change %)
NV	0	0
TTE-M3	8.7	42.1
TTE-P3	5.4	-17.5

**Table 5: AREA-AVERAGED PRESSURE LOSS COEFFICIENTS FOR LTE AIRFOILS**

Airfoil	Computation (Change %)	Measurements (area-averaged) (Change %)
LTE-25	13.0	58.0
LTE-50	40.2	63.2
LTE-75	63.0	101.7

The mass flow rate for synthesized airfoils normalized by NV airfoil mass flow rate is given in Table 6 for both the computation and the measurements. In CFD, the mass flow rate for the TTE-M3 airfoils decreased due to reduction in throat area, however remained the same for the TTE-P3 airfoil. For the LTE airfoils, mass flow essentially remained unchanged. In the measurements, the mass flow rate for TTE-M3 decreased, similar to the CFD and increased for TTE-P3 due to widening of the throat area. For the LTE airfoils, the flow rate progressively decreased with increase in the thickness of laminate repair.

**Table 6: NORMALIZED MASS FLOW RATE FOR TTE AND LTE AIRFOILS**

Airfoil	Normalized Mass Flow (Computation)	Normalized Mass Flow (Measurements)
NV	1.00	1.00
TTE-M3	0.95	0.97
TTE-P3	0.99	1.04
LTE-25	0.95	1.00
LTE-50	0.95	0.99
LTE-75	0.95	0.98

## CONCLUSIONS

The effect of profile modification of a nozzle guide vane due to repair on the performance of the turbine cascade was investigated by 2D cascade test experiments and numerical simulations. After a survey of various repair techniques used in the service industry, two representative repair schemes were selected for the study. Two profile parameters were determined, and five distinct parametric adjustments were made on the reference new vane. Two test profiles were developed by 3-degree tweaking of the TE of the NV airfoil. These were generated by mechanically bending the TEs towards the pressure side (TTE-M3) and the other towards the suction side (TTE-P3). The other three profiles were simulated by adding 25, 50 and 75% TE thicknesses on the NV airfoil towards the aft suction surface. The performance of the repaired profiles was compared with the reference NV performance profile.

The tweaking of the NV airfoil towards the pressure side decreased the throat area and produced higher exit Mach numbers, thereby producing higher shock losses and higher

total pressure losses in comparison with the NV profile. The tweaking towards the suction side increased the throat area and produced lower exit Mach numbers and thus lower total pressure losses. However, in an actual gas turbine engine, if the mass flow rates were limited because of flow in the other components, then these tweaked vanes may result in unchoked flow and consequent reduced power work from the stage.

The losses were significantly higher in comparison with the NV airfoil for the laminate repair profiles. The losses increased with the increase in the laminate repair thickness. This can be attributed to the increased losses in the wake and higher shock losses. This was aptly demonstrated in the case of 25% laminate repair thickness.

As well as shedding light on the performance of repaired profile models, the present study demonstrated, through CFD, that tweaking and laminate repairing of vanes would also shift the exit flow direction, and thereby affect the performance of the downstream rotor.

The present study provided sufficient evidence of performance changes, largely degradation, due to profile variation. A similar investigation on the profile modification due to surface distortion and repairs of the leading edge will be undertaken to provide recommendations to the service industry for developing repair guidelines.

## ACKNOWLEDGMENTS

The authors are thankful to the support staff of the Department of Mechanical and Aerospace Engineering, Royal Military College of Canada for the construction of the test rig. The authors would also like to express their gratitude to StandardAero for their tremendous support of this effort.

## REFERENCES

1. Woodason, R., "An Experimental Investigation of the Influence of Service Exposure on the Aerodynamic Performance of Transonic Turbine Vanes", MSc Thesis, Royal Military College, Kingston ON, Apr. 2009.
2. Edwards, R., Woodason, R., Asghar, A. and Allan, W.D.E., "Numerical Investigation of Real World Blade Profile Variations on the Aerodynamic Performance of Transonic Nozzle Guide Vane," GT2010-23461, Proceeding of ASME Turbo Expo 2009 Glasgow, UK, June 8-12, 2010.
3. Cohen, H., Rogers, G.F.C. and Saravanamutto, H.I.H., 1996, *Gas Turbine Theory*, 4<sup>th</sup> Ed., Longman Group Ltd, London, UK.
4. Wilson, D.G., 1984, *The Design of High-Efficiency Turbomachinery and Gas Turbines*, MIT Press, Cambridge, MA.
5. Farokhi, S., *Aircraft Propulsion*, Hoboken, N.J., John Wiley, 2009.
6. Aungier, R.H., 2006, *Turbine Aerodynamics: Axial-Flow and Radial-Inflow Turbine Design and Analysis*, ASME Press, New York.
7. Corriveau, D. and Sjolander, S.A., 2004, "Influence of Loading Distribution on the Performance of Transonic

- High Pressure Turbine Blades”, *J. Turbomachinery*, Vol. 126(2), pp. 288-296.
8. Li, S.-M, Chu, T.-L, Yoo, Y.-S., and Ng, W.F., 2004, “Transonic and Low Supersonic Flow Losses of Two Steam Turbine Blades at Large Incidences”, *J. Turbomachinery*, Vol. 126(4), pp. 966-975.
  9. Sonoda, T., Arima, T., Olhofer, M., Sendhoff, B., Kost, F., and Giess, P.-A., 2006, “A Study of Advanced High-Loaded Transonic Turbine Airfoils”, *J. Turbomachinery*, Vol. 128(3), pp. 650-657.
  10. Gostelow, J.P., Mahallati, A, Andrews, S.A. and Carscallen, W.E., “Measurement and Computation of Flowfield in Transonic Turbine Nozzle Blading with Blunt Trailing Edges”, ASME-GT2009-59686, *Proceeding of ASME Turbo Expo 2009*, Orlando, FL, June 8-12, 2009.
  11. Forster, V.T., 1964-65, “Turbine-Blading Development Using a Transonic Variable-Density Cascade Wind Tunnel”, *Proceedings of Institution of Mechanical Engineers*, Vol. 179, Pt 1., No. 6, pp. 155-195.
  12. Yasa, T., Paniagua, G, and Bussolin, A., 2007, “Performance Analysis of a Transonic High-Pressure Turbine”, *Proceedings of Institution of Mechanical Engineers*, Vol. 221, Part A: *J. Power and Energy*, pp. 769-778.
  13. Denton, J.D., and Xu, L., 1993, “The Trailing Edge Loss of Transonic Turbine Blades”, *J. Turbomachinery*, Vol. 112, No.2, pp. 277-285.
  14. Woodason, R., Asghar, A, and Allan, W.D.E., “Assessment of Flow Quality of a Transonic Turbine Cascade,” GT2009-60164, *Proceeding of ASME Turbo Expo 2009* Orlando, FL, USA, June 8-12, 2009.
  15. ANSYS CFX-Pre User’s Guide, Release 12.1, 2009, ANSYS Inc.
  16. Pandolfi, M. and D’Ambrosio, D., 2001, “Numerical Instabilities in Upwind Methods: Analysis and Cures for the ‘Carbuncle’ Phenomenon,” *Journal of Computational Physics*, Vol. 166, pp. 271-301.
  17. Menter, F.R., 1994, “Two-Equation Eddy Viscosity Turbulence Models for Engineering Applications”, *AIAA Journal*, vol. 32, No. 8, pp. 1598-1605.